Journal of Theoretical and Applied Physics (JTAP), Vol.16, No. 4, 162239 (1-7), 2022
Received 1 August 2022 ; Accepted 16 September 2022 ; [http://dx.doi.org/10.30495/jtap.162239]

Improved efficiency of a SiGe thin film solar cell structure using CNT charge collector layer

Homa Hashemi Madani[1]*, Mohammad Reza Shayesteh[1]*, Mohammad Reza Moslemi[2]

Abstract
In this study, a SiGe ($Si_{(1-X)}Ge_X$ x=0.1) thin film solar cell structure based on the carbon nanotube (CNT) charge collector is proposed and simulated. The addition of the CNT layer to the cell structure has been proven to change aspects of its physical characteristics, specifically the efficiency of the solar cell. Also, the performance of this cell is considering in present of two types of the CNT layers with sheet resistances of 128 $\Omega/\square$ and 76 $\Omega/\square$. According to the numerical simulation, the cell structure using CNT layer with sheet resistance of 128 $\Omega/\square$ has better performance parameters. The efficiency of proposed structure is 27.72%, which is higher than conventional structures without CNT layer. Furthermore, we optimize the structure by varying the thickness of the window, base, emitter, and substrate layers. The cell efficiency after this optimization reaches 30.63%. Finally, the optimal ratio of the width of the metal contact to the total width of the cell was calculated with the aim of reducing the shadowing loss effect. We show that total cell width in the presence of the CNT layer can be increased up to 1000 μm for the metal contact width of 50 μm, and an efficiency of 30.9% is obtained after this optimization.

Keywords
SiGe, thin film Solar cell, Carbon nanotube (CNT), Optimization.

[1] *Department of Electrical Engineering, Yazd Branch, Islamic Azad University, Yazd, Iran.*
[2] *Department of Electrical Engineering, Zarghan Branch, Islamic Azad University, Zarghan, Iran.*
***Corresponding author**: shayesteh@iauyazd.ac.ir

1. Introduction

One of the most interesting types of renewable energy is solar cell technology which appears to be the solution for environmental problems such as global warming. Photoelectric systems (PES) are expected to account for 25-30% of total power usage by 2030 [1]. Because of their quantity of raw ingredients, stability, fabrication technology advancement, and high efficiency, Si solar cells dominate the actual photovoltaic (PV) industry. Si solar cells presently account for almost 90% of the whole PV industry [2, 3]. It has been demonstrated that the SiGe material has superior properties to the Si material, including higher absorption coefficients at longer wavelengths, higher conductivity, lower cost of production, higher mechanical strength, suppression of high-intensity degradation of the solar cell under illumination, and the ability to change the band gap by changing the fraction of germanium [4]. In addition, higher photon absorption is projected to result in a considerable rise in photocurrent in the SiGe solar cell. On the other hand, a drop in open circuit voltage (V_{OC}) is seen as a result of a reduction in the SiGe band gap, which should be considered and avoided when optimizing cell behavior [5]. Due to their high mobility, manufacturing process compatibility, changeable lattice constant, and capacity to absorb light with wavelengths up to 1800 nm, SiGe and GaAs-SiGe dual-junction solar cells are frequently employed as bottom layers of multi-junction or tandem solar cells. Moreover, the smaller band gap and the lower surface recombination rate at higher concentrations of Ge in SiGe causes the higher light absorption coefficient, which can lead to the increase JSC in the cell structure. Therefore, according to these factors, we can expect high efficiency in SiGe-based solar cells [6–8].
CNTs and graphene are frequently regarded as environmentally acceptable and cost-effective materials for use in traditional solar cells [9], on the other hand, they are attractive prospects for a wide range of nanoscale electrical and photonic applications. The inclusion of nanotubes increases the mobility and conductivity of the carrier. Many researchers have concentrated on CNT applications in solar cells in order to lower overall resistance and shading impact. Because of its unique characteristics, such as semi-transparent conductivity, anti-reflective coating, and self-cleaning, CNTs are utilized as emitters or p-layers in Si-based solar cells [10–12]. Also, they have a variety of uses, including back, front, and buffer layers in solar cells, as well as photodetectors and light sensors [13]. This intriguing use is owing to graphene and nanotubes' excellent optical and electrical characteristics, which include strong electrical conduction, heat conduction, and high light transparency over a wide range of wavelengths. Because of their excellent physical qualities, they have also been employed to enhance the physical properties of other materials [14, 15]. Various studies have also been conducted on the effect of

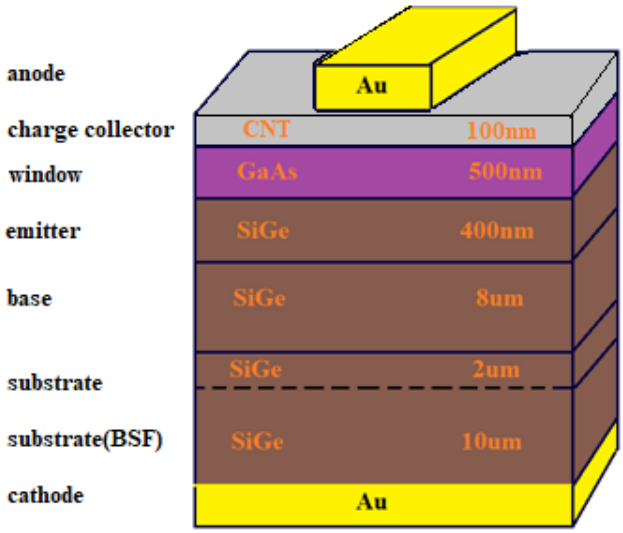

Figure 1. The proposed thin film SiGe solar cell structure with the CNT charge collector layer.

strain on the physical characteristics of CNTs [16–18].

According to reference [19], CNT-based 3D structures may transition from transparent to opaque materials with a relatively modest strain (0.4 percent). Reference [20] investigated the dependence of SWCNT phonon–phonon scattering rates on uniaxial tensile strain. It was demonstrated that the presence of strain changes the phonon–phonon scattering rates of SWCNTs by three orders of magnitude. A computer investigation on the structural features of SWCNTs revealed that the nanotubes can be altered to various situations and are extremely flexible for specific purposes [21]. Moreover, several studies have focused on the effect of nanomaterials on the performance of solar cells [22–25]. CNTs could deposit as a layers on the surface of solar cells. It was demonstrated that the light transmission of the CNT layer increases the power conversion efficiency and quantum efficiency of GaAs solar cells. They also demonstrated that putting a CNT layer on GaAs solar cells increases power conversion efficiency from

Table 1. CNT-based solar cell structures which was reported.

Structure	Efficiency%	Reference
CNT/Si	14.5-17%	11,12
CNT/GaAs	29.18%	13
CNT/n-Si	7.4%-14.1%	11,29,30
CZTS and CNT	11.31%	31
PVP/CZTS and CNT	15.21%	31
CNT/Provskite base	12.9%	32
CNT/DSSC based	1.98%	33
CNT/InGaP/GaAs	41.95%	34
PEDOT:pass-CNT	9.05%	35

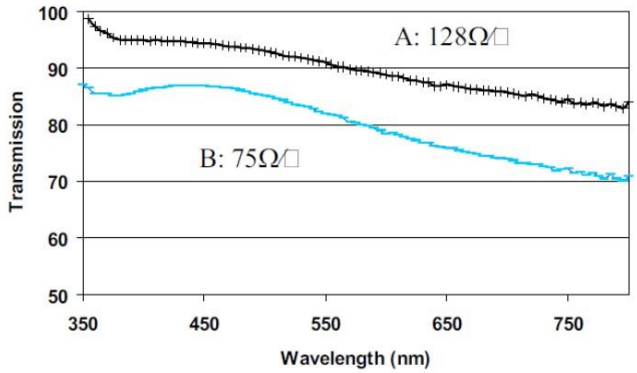

Figure 2. Transmission spectra of two different CNT layers [23].

26.04 to 29.18 percent [12, 26]. Furthermore, it has been demonstrated that the use of CNTs can increase the performance of solar cells [27]. It was discovered in this study that the addition of a thin CNT layer increases the efficiency of the solar cell due to its capacity to absorb more surface currents and have greater electrical conductivity. Furthermore, the usage of a CNT layer has been reported in a variety of other types of solar cells [28–34]. Table 1 lists some of the reported CNT-based solar cells.

The goal of this study is to optimize the proposed CNT-based SiGe thin film solar cell structure in order to improve its characteristic. The optimization is adjusted in stages, at the begin with choosing the appropriate CNT layer according to the sheet resistance and transparency, then comparing the results of the structure with and without CNT layer, finally we optimize the thickness of the layers and calculate the optimal ratio of the width of the metal contact to the total width of the cell.

The remainder of this work is structured as follows. Section 2 discusses the proposed SiGe thin film solar cell structure based on CNTs. In section 3, we give the theoretical model that was used to simulate the device. Section 4 discusses the simulation and optimization of the cell structure findings and debates. Finally, in Section 5, we bring this study to a close.

2. The proposed CNT-based SiGe thin film solar cell structure

The schematic of the basic structure of a CNT-based SiGe thin film solar cell is shown in Figure 1. The solar cell heterostructure consists of a 12-μ-thick SiGe layer as the substrate that include a 10μm back surface field(BSF), and 2μm substrate, 8-μ-thick SiGe layer as the base layer, a 400-nm-thick SiGe layer as the emitter layer, a 500-nm-thick GaAs layer as the window layer, and a 100-nm-thick semi-transparent CNT network layer as the charge collector, all of these thickness would be optimized to reach the best solar cell performance. Also, gold layer with a thickness of 100nm is used as the electrodes. Single-walled carbon nanotubes (SWNTs) are one-dimensional

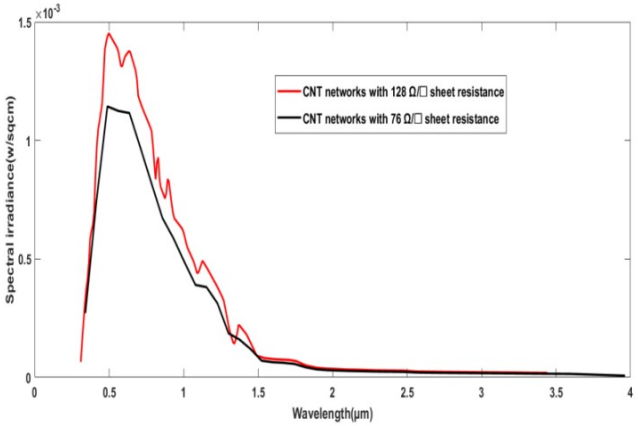

Figure 3. Modified spectrum in the simulation of CNT layers with sheet resistances of 128 and 76Ω/□.

and narrow-band conductors. CNTs are semiconductors with a diameter of about 1 nanometer and a length of several micrometers. SWCNT networks have been successfully used in many electronic devices as an alternative to transparent conductive oxides (TCOs), because of their difficulty of manufacturing and the cost of producing for high quality TCOs, the CNTs are suitable replace to these transparent conductors [35]. Finding a more conductive and transparent layer as a top layer in the solar cellscould help to improve the overall cell performance. Using CNTs can reduce the surface area of solar cells covered by the top metal fingers, on the other hand, we can increase the distance between the metal mesh lines witch collect current. Advantage of using the transparent CNT network layer as the charge collector could describe as: create a low-resistance path for the carriers, reducing the series resistance of the cell, and reducing the number of front electrodes and the shading effect. All of these can improve the solar cell performance. The layers thickness and doping profile of the structure is listed in Table 2.

Table 2. Layer thickness and doping profile.

Layer	Material	Thickness μm	Doping cm^{-2}
Electrode	Au	0.1	-
Semitransparent	CNT	0.1	-
Window	GaAs	0.5	P type-1e18
Emitter	SiGe	0.4	P type-1e18
Base	SiGe	8	N type-1e17
Substrate	SiGe	2	N type-1e18
BSF	SiGe	10	N type-3e18

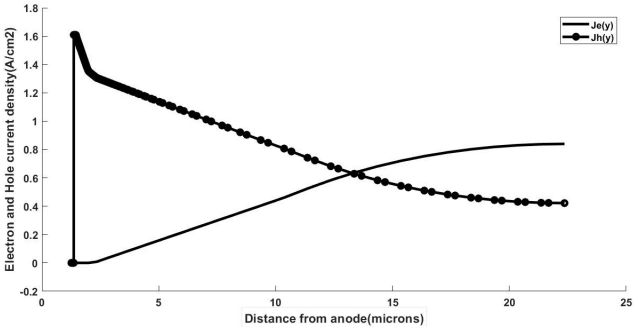

Figure 4. Electron and hole current density inside the proposed cell structure.

3. Theoretical modeling

For simulation of the solar cell structures, the dynamics of the carrier can be described by the one-dimensional equations of drift-diffusion, the current continuity equations and the Poisson equation. The Poisson equation is shown below:

$$\nabla^2 V = \frac{q}{\varepsilon_r \varepsilon_0}(n - p - N) \tag{1}$$

where V is the potential, q is the initial charge, ε_r and ε_0 are the relative dielectric constant and the vacuum dielectric constant, respectively. n and p are the electron and hole concentration, respectively. The drift-diffusion equation and the current continuity equation are expressed as follows:

$$J_n = -qn\mu_n \nabla V + qD_n \nabla n$$

$$J_p = -qp\mu_p \nabla V - qD_p \nabla p \tag{2}$$

where J_n and J_p are the electron and hole current density, respectively. μ_n and μ_n are the electron and hole mobility and D_n and D_p are the electron and hole diffusion constant, respectively.

$$\frac{1}{q}\nabla \cdot J_n - R_n + G_n = 0$$

$$-\frac{1}{q}\nabla \cdot J_p - R_p + G_p = 0 \tag{3}$$

where G_n and G_p are the electrons and hole generation rate because of light illumination. R_n and R_p are the recombination rate of electrons and holes, respectively [36–38].

Also, the charge carrier statistics in the CNTlayer can be described as follows [13]:

$$p - n = sign(E_D - E_F)\frac{1}{\pi\hbar^2 v_F^2}(E_F - E_D)^2 \tag{4}$$

Where p and n are the holes and the electrons density in the CNT layer, E_D and E_F are the Dirac point and the Fermi level of the CNT layer, respectively. Also, $\hbar$ is the reduced Planck's constant and v_F is the Fermi velocity in the CNT layer. The

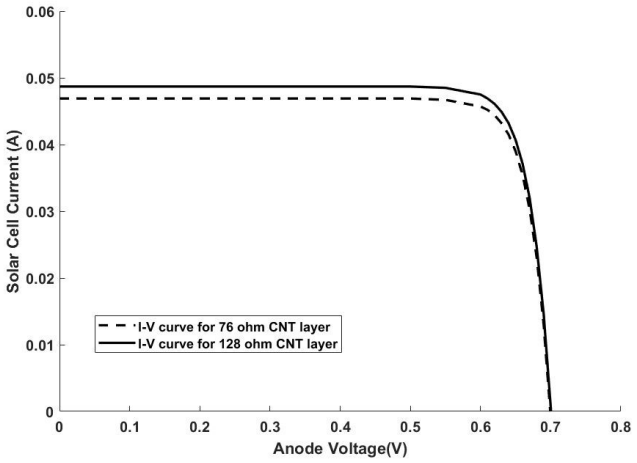

Figure 5. The $I-V$ curves of cells with different sheet resistances of the CNT layer.

height of the junction barrier in the CNT/SiGe can be inferred by matching the JV curves (in the dark mode) in the Schottcky CNT/SiGe diode:

$$J = J_0 e^{(\frac{qV}{N_{IF}KT}-1)} \tag{5}$$

Where K is Boltzmann's constant, N_{IF} is the ideal factor of the junction, and T is temperature. Based on the thermionic-emission theory:

$$V_{OC} = \frac{N_{IF}KT}{q}\ln(\frac{I_L}{I_0}+1) \tag{6}$$

In general the power delivered from a power source can be $P = IV$. If the current density of J is used in this relation, we obtain the power density ($P_d = JV$). The maximum power density occurs somewhere between $V = 0$ (short circuit) and $V = V_{oc}$ (open circuit) at V_m voltage. The corresponding current density is called J_m, so the maximum power density is $P_m = J_m V_m$. The efficiency of a solar cell is as follows [39]:

$$P_{max} = V_{OC} I_{SC} FF \tag{7}$$

FF is fill factor that used to describe a solar cell performance. The fill factor can be defined as follows:

$$FF = \frac{V_{OC} - \ln(V_{OC}+0.72)}{V_{OC}+1} = \frac{I_m V_m}{I_{SC} V_{OC}} \tag{8}$$

Using FF we can write the efficiency as follow:

$$\eta = \frac{V_{OC} I_{SC} FF}{P_{in}} = \frac{P_{max}[W]\times 100}{1000[Wm^{-2}]\times CellArea[m^2]} \tag{9}$$

where V_{OC} and I_{SC} are the open circuit voltage and short circuit current respectively and P_{in} the input light power density, which is assumed to be 1000 Wm^{-2} in our simulation.

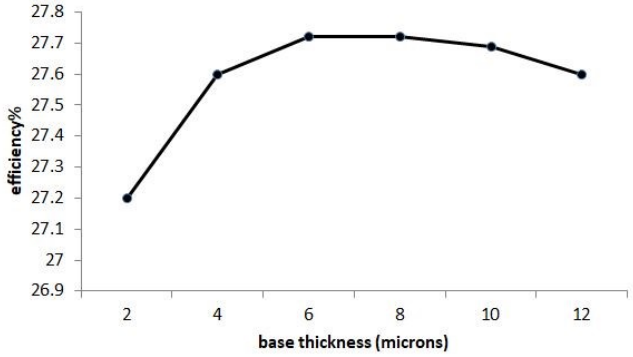

Figure 6. Efficiency of the solar cell for different base layer thicknesses.

4. Results and discussions

In this part, the proposed structure of CNT-based SiGe thin film solar cell was simulated and the performance characteristics of cells such as J_{sc}, V_{oc}, FF, P_{max} and efficiency are calculated. The parameters which used in our simulation are given in Table 3 and Table 4.

In the next step, we intend to simulate the proposed structure in presence of two different types of CNTs, then calculate and compare the performance parameter of the cells. The two types of CNTs were fabricated by the Canadian Institute of Microstructural Sciences with sheet resistances of 76 and 128 $\Omega/\square$ [10]. This layer is used as a charge collector in the cell structure and creates a low resistance path for the carrier to reach the top contact. In this heterogeneous CNT network, 1/3 of the nanotubes are metal and 2/3 of them are semiconductors.

In this simulation, we modeled the input power spectrum of the cell using the information of the CNT layer transmission spectrum for 128 and 76 $\Omega/\square$ sheet resistances [13]. Figure 2 shows the transmission spectra of two different CNT layers with resistances 128 and 76 $\Omega/\square$. Also, the modified AM1.5 spectrum is shown in Figure 3 by considering the transmission coefficient of two different CNT layers with different sheet resistances 128 and 76 $\Omega/\square$, which we use as the input power spectrum in the simulation.

For choosing the suitable CNT layer, the proposed cell structure is simulated with two types of CNT layers with different sheet resistances, 76 and 128 $\Omega/\square$, and the voltage-

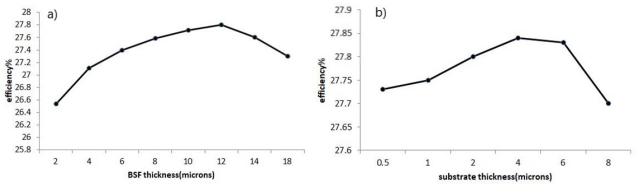

Figure 7. (a) Efficiency of the solar cell for varying the substrate thickness,(b) Efficiency of the solar cell for varying the BSF layer thickness.

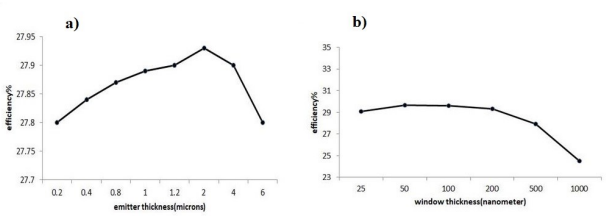

Figure 8. (a) Efficiency of the solar cell for different emitter layer thicknesses,(b) Efficiency of the solar cell for different window layer thicknesses.

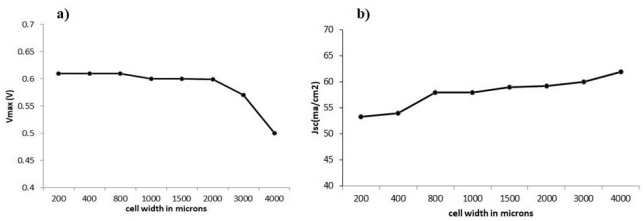

Figure 9. (a) Maximum cell voltage (Vmax) curve for changes in the cell width,(b) Short circuit current density for changes in the cell width.

current characteristic and efficiency in both cases are compared. Higher sheet resistance means lower density of metal nanotubes and consequently more transparency of the layer. On the other hand, the small sheet resistance means higher metallic nanotube concentration which makes the CNT layer more opaque, and hence the absorption in the active layer decreases and can reduce the performance of the whole cell. Figure 5 shows the $I-V$ characteristics using two types of CNT layers with different Sheet resistances. According to these results, the CNT layer with sheet resistance of 128 $\Omega/\square$ leads to a better result and higher efficiency. For further comparison, the characteristics of the conventional SiGe solar cell structure without the CNT layer are shown.

As mentioned earlier, in these structures the CNT layer plays an important role in the cell performance. The rapid transfer of electron-hole pairs which was created in the absorber layer to the contact well done by the CNT layer.

Figure 4 shows the current density of electrons and holes in the proposed cell structure in Y direction (solar cell depth) and the place of zero distance is the top electrode of cell. As shown in the figure, the electron current density near the CNT layer is the maximum value. Indeed, the charge carriers were created in the absorber layer are separated and sent to the contacts through the CNT layer. This is the important role of the CNT layer in the solar cell performance.

Next, for the proposed CNT-based SiGe solar cell structure in the presence of a CNT layer with a sheet resistance of 128 $\Omega/\square$ as the charge collector layer, we optimize the thickness of the base layer and try to find the best thickness of this layer. Figure 6 shows the cell efficiency for changes in the base layer thickness from 2 microns to 12 microns. As can be seen, the efficiency of the solar cell is maximized for a thickness of 6 microns. Increasing the base thickness can increase the series resistance of the path, so the Base layer thickness should be optimize.

For the next step, we consider the thickness of the base layer to be constant and equal to 6 μm and try to find the best thickness for substrate layer. The total substrate thickness was considered 12 μm in the primary structure, which includes 2 μm as the substrate and 10 μm SiGe as the BSF layer. This difference between concentration in substrate profile make carrier push forward and prevent carrier recombination in back contact and then as can be seen from Figure 7(a) the best performance was obtained for the BSF layer in 12 μm. The figure 7(b) shows the best thickness for the substrate layer is 4 μm.

The window and emitter layer thickness also was optimized and Figure 8 shows the results. As shown in Figure 8(a), the optimized thickness for emitter layer is 2 μm and the optimized thickness for window layer is 50 nm. If the p-n junction in the solar cell be close to the surface, more light is absorbed in the base region and more electron-holes pairs are produced in the base region, so decreasing in window layer could increase the cell efficiency. On the other hand, increasing the emitter thickness could increase the active layer thickness and have a good impact on cell efficiency, but finding the opti-

Table 3. Parameters of CNT layer [13].

Characteristics	Value
Band gap E_g (eV)	0.026
Electron affinity X_e (eV)	5.8
Relative permittivity ε_r(F cm^{-1})	5.4
Electron, Hole mobility μ_n,μ_p(cm^2/Vs)	13889 (for 128$\Omega/\square$)
Electron, Hole mobility μ_n,μ_p(cm^2/Vs)	8138.2 (for 76$\Omega/\square$)
Conduction band effective density of states (cm^{-3})	3×10^{17}
Valence band effective density of states (cm^{-3})	3×10^{17}

Table 4. Material parameters used in our simulation [12, 39, 40].

layer identifier	Window GaAs	Absorber SiGe(x=0.1)
E$_g$(eV)	1.42	1.08
Affinity(eV)	4.07	4.045
Permittivity ε_r (Fcm^{-1})	13.1	12.15
μ_n(cm^2/Vs)	8000	1000
μ_p(cm^2/Vs)	400	500
Conduction band effective density of state N$_c$(cm^{-3})	4.7×10^{17}	2.62×10^{19}
Valence band effective density of state N$_v$(cm^{-3})	$7\times10^{18}18$	0.996×10^{19}

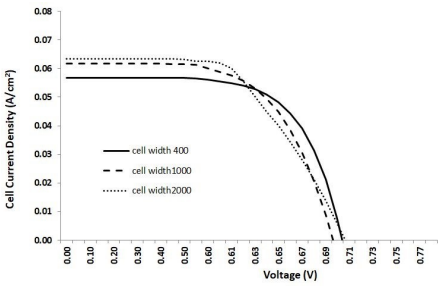

cell width (um)	FF
200	84.6
400	83.7
800	82.93
1000	82.33
1500	80.4
2000	77.3

Figure 10. The $I-V$ curves for changes in the cell width.

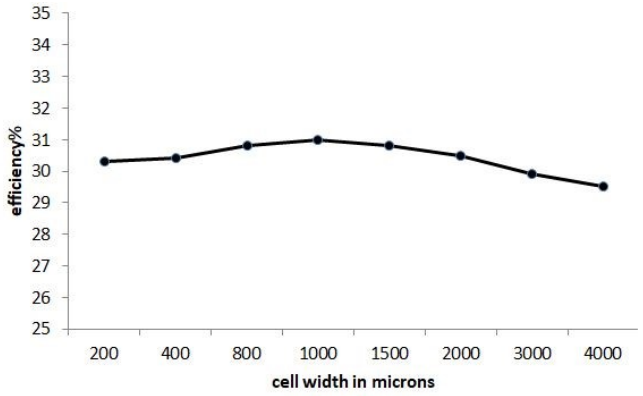

Figure 11. The Efficiency curve for changes in the cell width.

mize thickness is necessary because the excessive increase in thickness leads to a decrease in cell efficiency. After all layer thickness optimization the solar cell efficiency reach to 30.63%.

In the final part, we optimize the ratio of the width of the metal contact to the total width of the cell. In the initial structure, the width of the top contact of the cell was considered to be 50 μm and the total width of the cell was considered to be 200 μm, it means 25% of the cell was covered by the top contact. In order to reduce the shadowing loss effect, we change the total width of the cell from 200 to 4000 μm, while the width of the top metal contact in all stages of the simulation is considered a constant value of 50 μm. The short-circuit current density increases with increasing cell width. Also when the cell width increases, the cell open circuit voltage will increase slightly. This small increase in open circuit voltage is due to the generation of more charge carriers in the cell structure.

Figure 9(a) shows the maximum cell voltage (V_{max}) curve for changes in cell width. As can be seen, the V_{max} of the cell will decrease significantly as the cell width increases. As the width of the cell increases, the distance traveled by the charge carriers to reach the top contact increases and therefore the voltage drop due to series and shunt resistance increases and this reduces maximum cell voltage. Decreasing V_{max} reduces the maximum power (P_{max}) in larger cell width. Figure 9(b) shows the short-circuit current density increases with increasing cell width. This result is acceptable because by increasing the cell width and keeping the contact width constant, the percentage of cells covered by the contact decreases and hence the absorption due to the contact decreases. Although the current is gradually increasing, but finally the dominant effect of reducing the V_{max} is reducing the cell efficiency. Therefore, to increase cell efficiency, the cell width cannot be increased too much. Because for large amounts of cell width, the V_{max} value decreases and hence the P_{max} decreases.

Figure 10 shows the cell fill factor (FF) for changes in the cell width. As the figure shows, increasing the cell width increases the internal resistance of the cell and thus decreases the FF. Reducing FF can also reduce the V_{max} and the maximum available cell power. According to the obtained results the FF value in 1000 μm cell width is 82.33%.

As can be seen in Fig 11 the efficiency of solar cell is almost constant because the short circuit current density is increasing slightly and after 1000 μm the decreasing in V_m causes to decrease the efficiency.

5. Conclusion

In this study, a CNT-based SiGe thin film solar cell structure has been proposed. We first simulated a CNT-based SiGe solar cell in presence of two different CNT layer with sheet resistance 128 and 76 $\Omega/\square$. We showed that the CNT layer with higher sheet resistance and greater transparency is more suitable for this structure and the efficiency of the proposed structure was 27.72%. Then, by optimizing the thickness of the cell layers, we have increased the efficiency of the proposed structure to 30.63%. Finally, the optimal ratio of the width of the top metal contact to the total width of the cell was calculated. We showed by using the CNT layer as the charge collector, we can increase the distance between the metal contacts without changing their thickness to reduce the shadowing loss effect. In this proposed cell structure, we obtained an efficiency of 30.9% for a total cell width of 1000 μm and a width of 50 μm for the top contact.

Conflict of interest statement:

The authors declare that they have no conflict of interest.

References

[1] L. F. Kozin. *Ukraine springer*, **2**:4, 2010.

[2] T. Sugiura, S. Matsumoto, and N. Nakano. *IEEE Journal Of Photovoltaics*, **10**:1, 2020.

[3] P. Procel, G. Yang, O. Isabella, and M. Zeman. *IEEE Journal Of Photovoltaics*, **9**:374, 2019.

[4] R. Pandey and R. Chaujar. *Solar Energy*, **135**:242, 2016.

[5] S. Michael, A. D. Bates, and M. S. Green. *Conference Record of the Thirty-first IEEE Photovoltaic Specialists Conference*, :8505061, 2005.

[6] X. Zhao, D. Li, T. Zhang, B. Conrad, L. Wang, A. H. Soeriyadi, J. Han, M. Diaz, A. Lochtefeld, A. Gerger, I. Perez-Wurfl, and A. Barnett. *Solar Energy Materials and Solar Cells*, **159**:86, 2017.

[7] A. B. Poungoue Mbeunmi, M. El-Gahouchi, R. Arvinte, A. Jaouad, R. Cheriton, M. Wilkins, C. E. Valdivia, K. Hinzer, S. Fafard, V. Aimez, R. Arés, and A. Boucherif. *Solar Energy Materials and Solar Cells*, **217**:110641, 2020.

[8] P. Ca no, M. Hinojosa, H. Nguyen, A. Morgan, D. F. Marrón, I. García, A. Johnson, and I. Rey-Stolle. *Solar Energy Materials and Solar Cells*, **205**:110246, 2020.

[9] T. Mahmoudi, Y. Wang, and Y.-B. Hahn. *Nano Energy*, **47**:51, 2018.

[10] H. Hanaei, M. K. Assadi, and R. Saidur. *Renewable and Sustainable Energy Reviews*, **59**:620, 2016.

[11] X. Zhao, H. Wu, L. Yang, Y. Wu, Y. Sun, Y. Shang, and A Cao. *Carbon*, **147**:164, 2019.

[12] K. J. Singh, T. J. Singh, D. Chettri, and S. K. Sarkar. *Optik*, **135**:256, 2017.

[13] H. Liu, P. Liu, L. Bian, C. Liu, Q. Zhou, and Y. Chen. *Superlattices and Microstructures*, **112**:470, 2017.

[14] I. Burmistrov, N. Gorshkov, I. Ilinykh, D. Muratov, E. Kolesnikov, E. Yakovlev, I. Mazov, J.-P. Issi, and D. Kuznetsov. *Composites Science and Technology*, **147**:71, 2017.

[15] X. Zheng, Y. Huang, S. Zheng, Z. Liu, and M. Yang. *Journal of Thermoplastic Composite Materials*, **32**, 2019.

[16] C. Zhu, A. Chortos, Y. Wang, R. Pfattner, T. Lei, A. C. Hinckley, I. Pochorovski, X. Yan, J. W. F. To, J. Y. Oh, J. B. H. Tok, Z. Bao, and B. Murmann. *Nature Electronics*, **1**:183, 2019.

[17] L. Hu, W. Yuan, P. Brochu, G. Gruner, and Q. Pei. *Applied Physics Letters*, **94**:161108, 2009.

[18] A. Darvishzadeh, N. Alharbi, A. Mosavi, and N.E. Gorji. *Physica B: Condensed Matter*, **543**:14, 2018.

[19] Y. Li, P. S. Owuor, Z. Dai, Q. Xu, and R. V. Salvatierra and. *Journal of Materials Chemistry C*, **7**:1927, 2019.

[20] Y. Chu, P. Gautreau, T. Ragab, and C. Basaran. *Computational Materials Science*, **112**:87, 2016.

[21] N. Karachi, M. Emadi, and M. Servatkhah. *Journal of Optoelectronical Nanostructures*, **4**:99, 2019.

[22] P. Krogstrup, H. I. Jørgensen, M. Heiss, O. Demichel, J. V. Holm, M. Aagesen, J. Nygard, and A. Fontcuberta i Morral. *Nature Photonics*, **7**:306, 2013.

[23] I. Åberg, G. Vescovi, D. Asoli, U. Naseem, J. P. Gilboy, C. Sundvall, A. Dahlgren, K. E. Svensson, N. Anttu, M. T. Björk, and L. Samuelson and. *IEEE Journal of photovoltaics*, **6**:185, 2015.

[24] K. Nakayama, K. Tanabe, and H. A. Atwater. *Applied Physics Letters*, **93**:121904, 2008.

[25] W. Jie, F. Zheng, and J. Hao. *Applied physics letters*, **103**:23311, 2013.

[26] K. J. Singh and T. J. Singh. *IOP Conference Series: Materials Science and Engineering*, , 2017.

[27] S. N. Jafari, A. Ghadimi, and S. Rouhi. *The European Physical Journal Applied Physics*, **88**:20401, 2019.

[28] X. Huang, R. Xie, H. Sugime, and S. Noda. *Applied Surface Science*, **542**:148682, 2021.

[29] R. Xie, H. Sugime, and S. Noda. *Carbon*, **175**:519, 2021.

[30] Z. Shadrokh, Sh. Sousani, S. Gholipour, and Y. Abdi. *Solar Energy*, **201**:908, 2020.

[31] M. NahidReza. *10th International Electrical and computer Engineering Conference, IEEE*, , 2018.

[32] S. Widodo and M. N. Hidayat. *Energy Procedia*, **68**:37, 2015.

[33] B. Farhadi and M. Naseri. *Optik*, **127**:6224, 2016.

[34] K. K. Markose, M. Jasna, P. P. Subha, A. Antony, and M. K. Jayaraj. *Solar Energy*, **211**:158, 2020.

[35] P. Glatkowski, E. Turevskaya, D. Britz, D. Rich, M. DiCologero, T. Kelliher, J. Sennott, D. Landis, R. Braden, P. Mack, and J. Piche. *34th IEEE Photovoltaic Specialists Conference (PVSC)*, :11152130, 2009.

[36] J. W. Slotboom. *Electronics Letters*, **5**:677, 1969.

[37] H. K. Gummel. *IEEE Transactions on Electron Devices*, **11**:455, 1964.

[38] Kh. J. Singh, N. B. Singh, and S. K. Sarkar. *Journal of Computational Electronics*, **1**:288, 2015.

[39] M. A. Green. *Solid-State Electronics*, **24**:788, 1981.

[40] S. Kasap (Editor) and P. Capper (Editor). *Springer Handbook of Electronic and Photonic Materials*. Springer Handbooks, 2th edition, 2017.